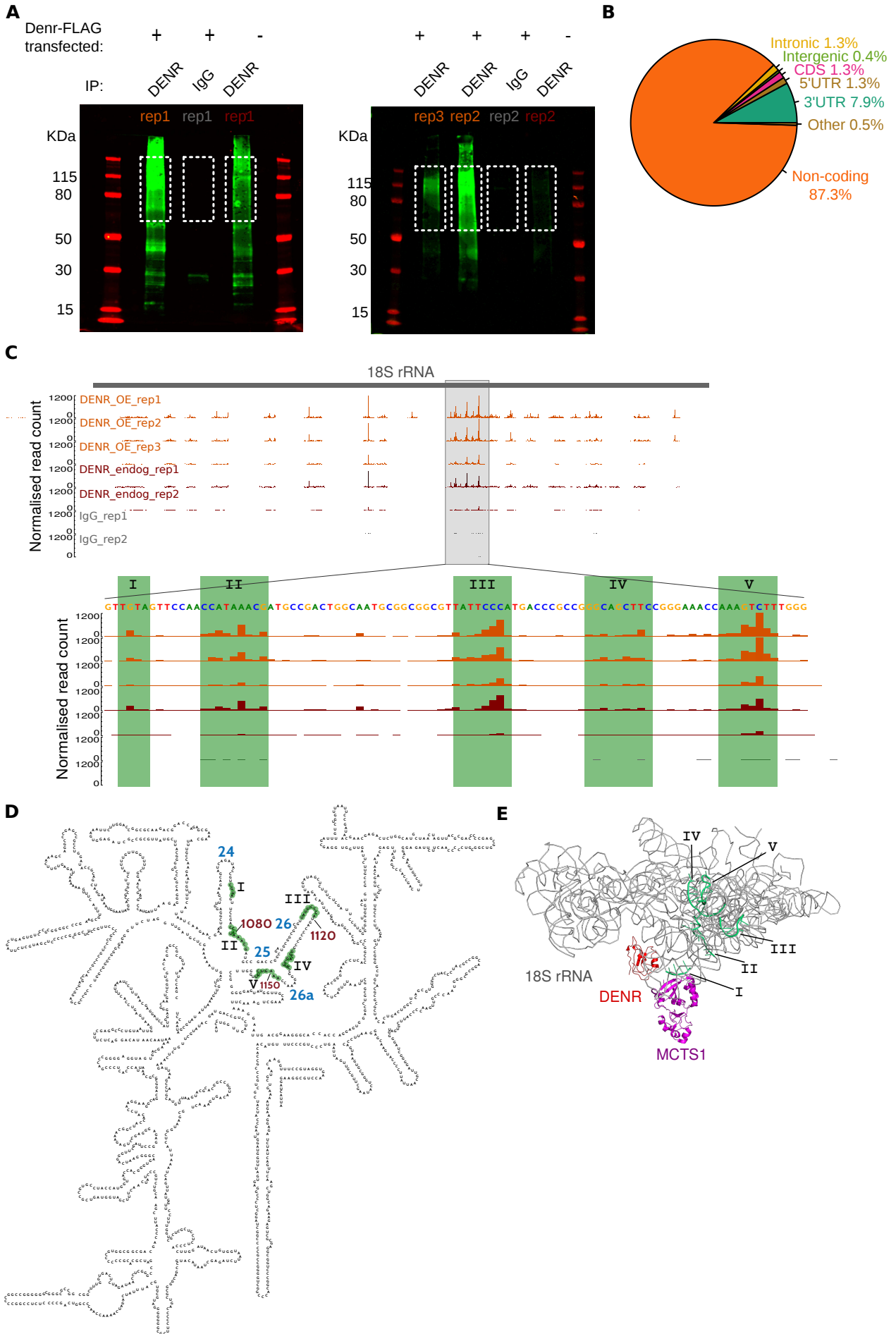
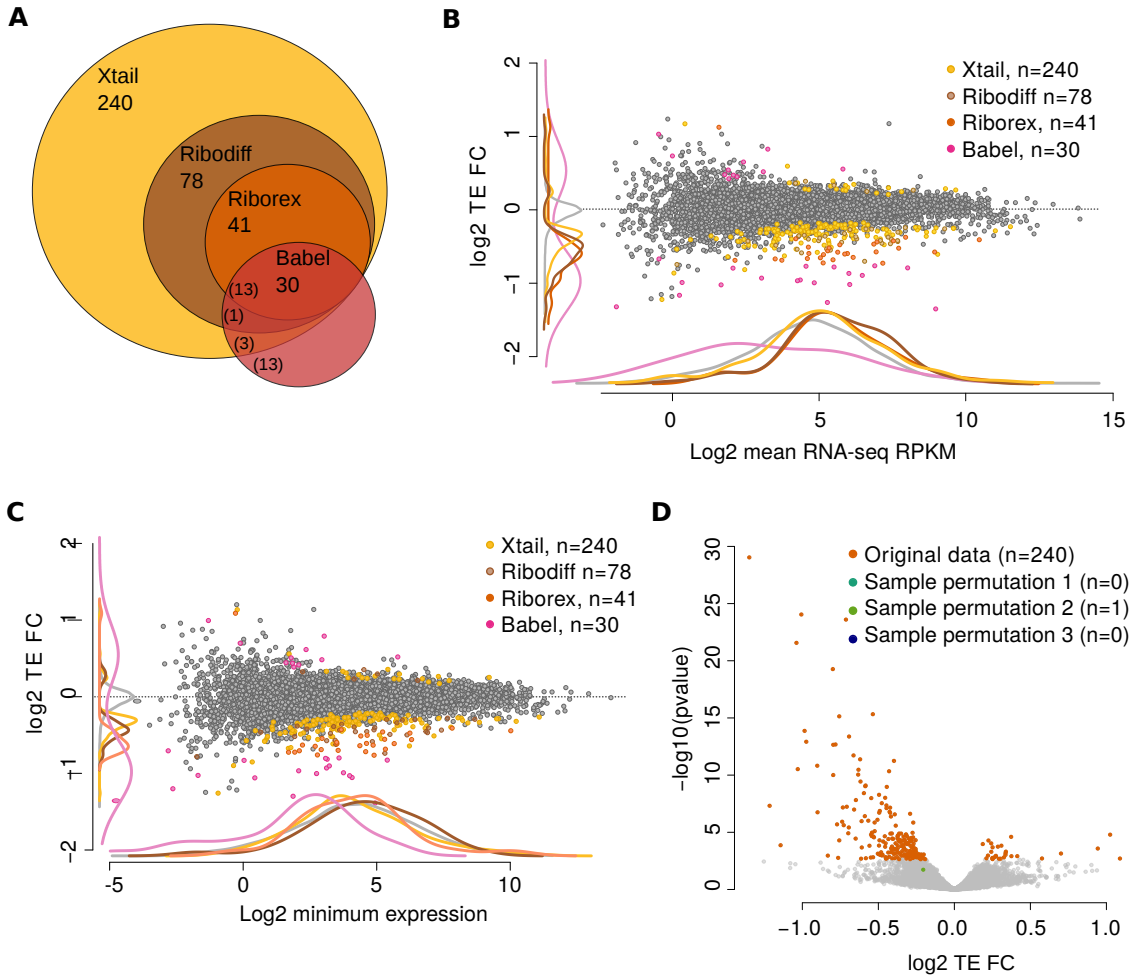


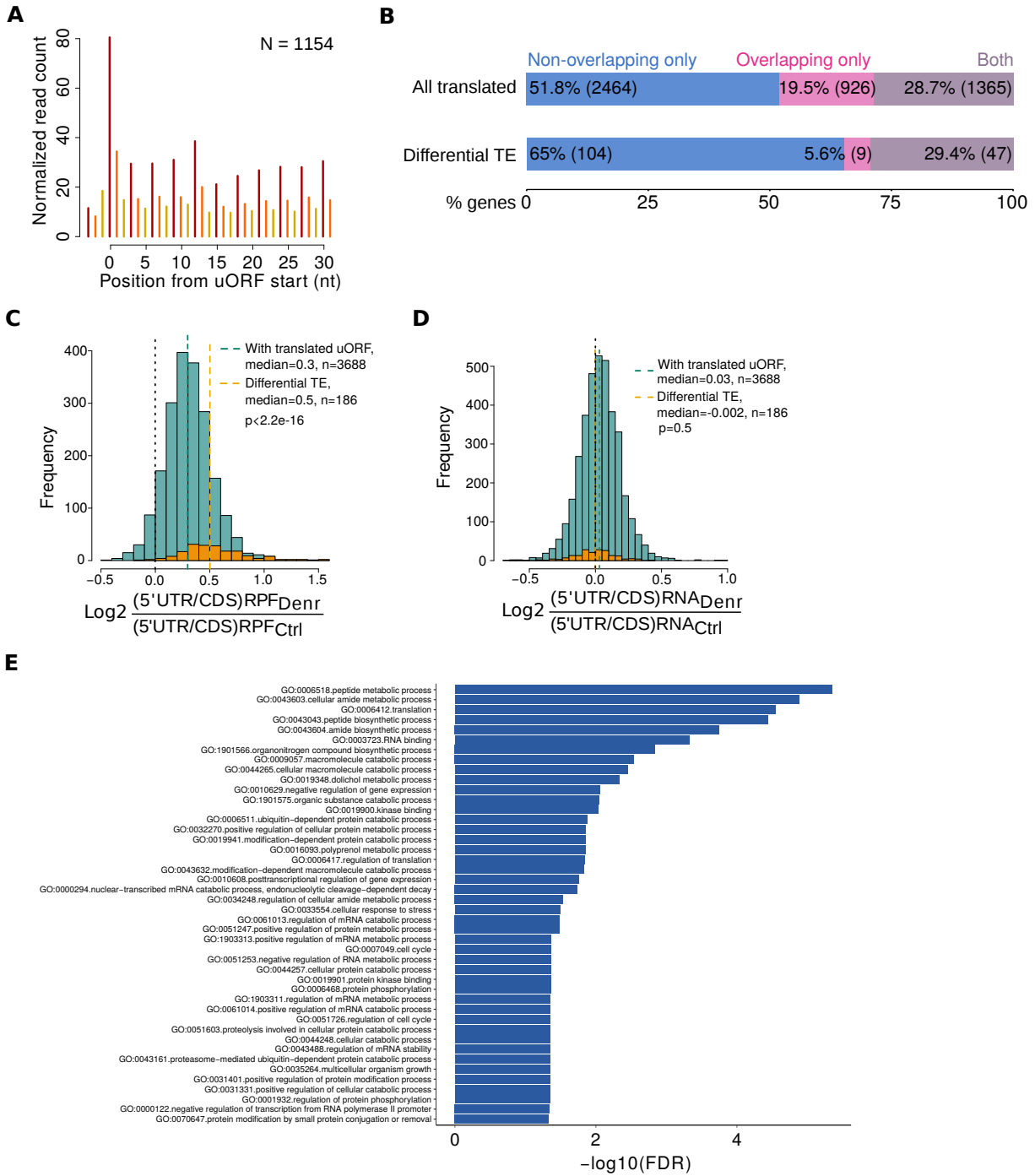
Supplementary Figure 1. Ribosome profiling in *Denr* knockdown NIH3T3 mouse fibroblasts. **A)** Read length distribution for ribosome footprint (RPF-seq) and mRNA (RNA-seq). Footprint length distribution peaks sharply at 29-30 nt, whereas RNA-seq reads showed a broader distribution, as expected. **B)** Read mapping to transcript features. RPF-seq and RNA-seq compared to a distribution expected from the relative feature size (grey). In both *Denr* Kd and control cells, RPF-seq but not RNA-seq reads were depleted from 3' UTRs and enriched on the CDS. A significant amount of reads also mapped to 5' UTRs. **C)** Meta-gene analysis of the footprints' ribosome A-site positions relative to the start and stop codons of the transcripts. Read density at each position was averaged across genes with a single protein-coding isoform, with a CDS RPF RPKM > 5 and longer than 400 nt (n = 3141). This analysis revealed the trinucleotide periodicity of RPF-seq, but not RNA-seq, reads. **D)** Tables of Spearman correlation coefficients between samples for normalized CDS reads. On the right, one representative example of normalised CDS reads correlation between replicate samples. **E)** RPKM values for CDS-mapping RPF-seq read counts for *Denr* (left), *Mcts1* (middle), and *Eif2d* (right). Each dot corresponds to a sample and replicate and error bars indicate mean \pm sd. **F)** Metagene analysis of normalized RPF-seq read counts across 5' UTRs. 5' UTRs were scaled to forty windows of equal size and RPF signal was averaged within each window and across genes. *Denr*-deficient cells showed an accumulation of ribosome footprints on the 5' UTR – possibly due to the presence of translated uORFs – that can explain the change in relative 5' UTR shown in Fig. 1E, and indicative of a translational landscape remodelling. **G)** Histogram of 5' UTR-to-CDS mRNA abundance ratios (from RNA-seq) between *Denr* Kd and control cells, using same genes as in Fig. 1E. In contrast to translation, relative 5' UTR transcript levels did not change between conditions (median = 0.03, p = 0.09).



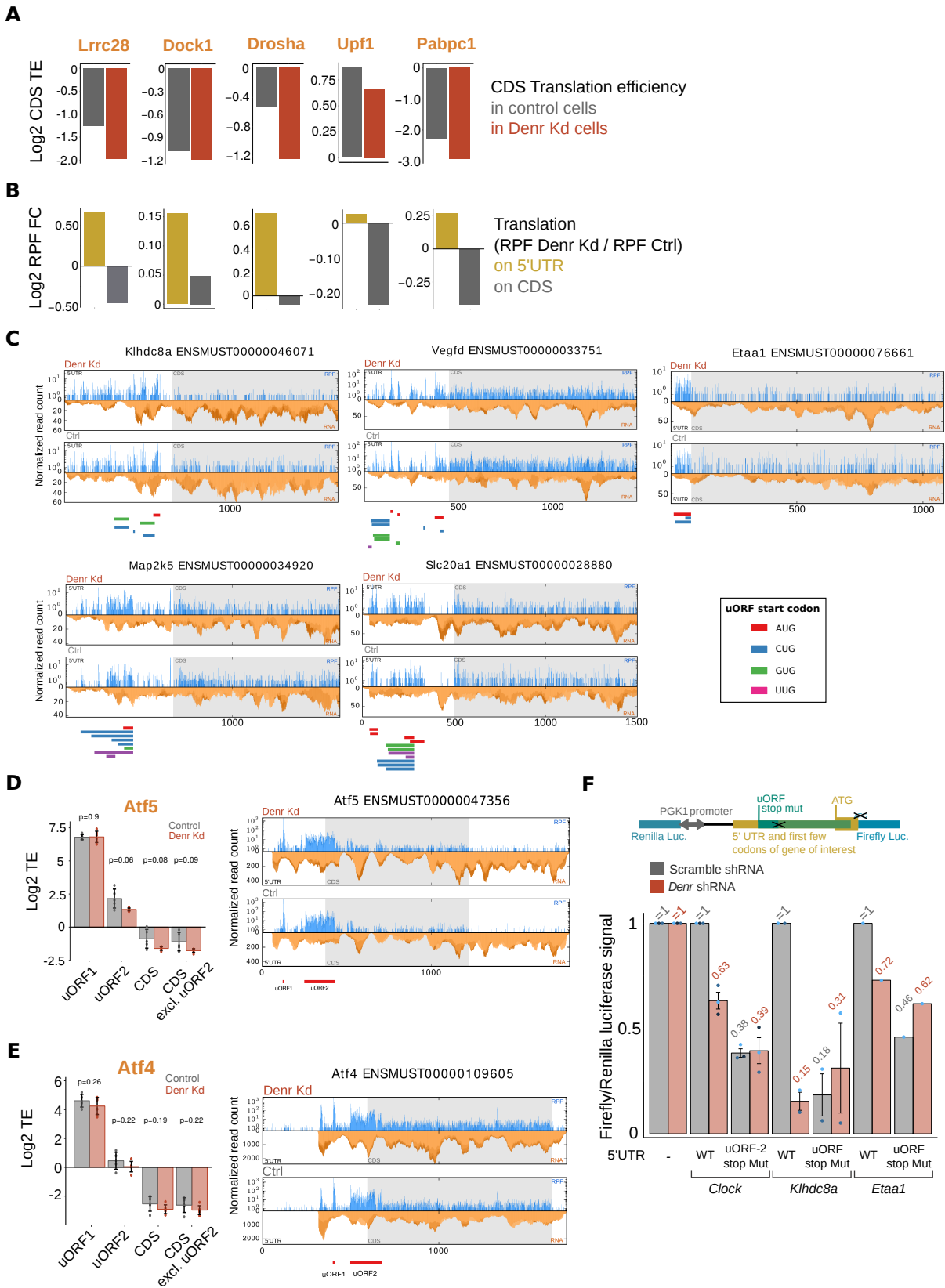
Supplementary Figure 2. DENR-MCTS1 iCLIP in NIH3T3 cells. **A)** Li-Cor image of infrared adaptor-ligated protein-RNA complexes. The region within the white rectangle – likely representing RNA-bound DENR:MCTS1 (together ~50KDa) complexes – was excised and used for library preparation. NIH3T3 cells overexpressing DENR were used in triplicate for iCLIP experiments; non-overexpressing cells in duplicate, and an IgG IP was done in duplicate, as a negative control. **B)** Mapping summary of iCLIP experiments in cells overexpressing DENR. Sections represent percentage of cDNA read counts per kilobase uniquely mapping to the regions indicated. **C)** Overview of high-confidence binding peaks mapping within the 18S rRNA (top), and zoom into the region with the five most prominent peaks (bottom), located within helices 24-26. Plots were generated with Biodalliance genome visualisation tool (biodalliance.org). **D)** Secondary structure of 18S rRNA; in green, the five most prominent binding sites highlighted in C. **E)** Crystal structure of DENR:MCTS1 in complex with 18S rRNA (PDB: 5VYC; from Lomakin et al. 2017, ref. 32), highlighting the five most prominent binding sites, as in C,D.



Supplementary Figure 3. Comparison of algorithms for differential translation efficiency analysis. **A)** Venn diagram of differential TE genes detected by Xtail (n=240), RiboDiff (n=78), Riborex (n=41) or Babel (n=30) with an FDR < 0.1. The analysis showed agreement among the first three algorithms, with Xtail detecting the largest number of significant cases. **B)** Scatter plot with marginal densities of average mRNA abundance vs. TE fold change (*Denr* Kd/Ctrl), with differential TE genes highlighted for each algorithm. For cases detected by several algorithms, the genes are coloured according to the method detecting fewer genes, and density lines correspond to the distribution of all detected cases. The majority of Xtail, RiboDiff and Riborex detected genes showed decreased TE in *Denr* deficient cells as expected, and spanned all levels of expression, whereas Babel detected similar numbers of up- and downregulated TE genes and showed a bias for lowly expressed genes. **C)** As B, but showing minimal expression in the x-axis, i.e. the lowest value among all RNA-seq and RPF-seq replicates. **D)** Volcano plot of differential TE genes detected by Xtail on the original data (n=240) and on three condition-shuffled datasets. Sample permutation yielded nearly no significant genes, indicating low false positive detection by Xtail.

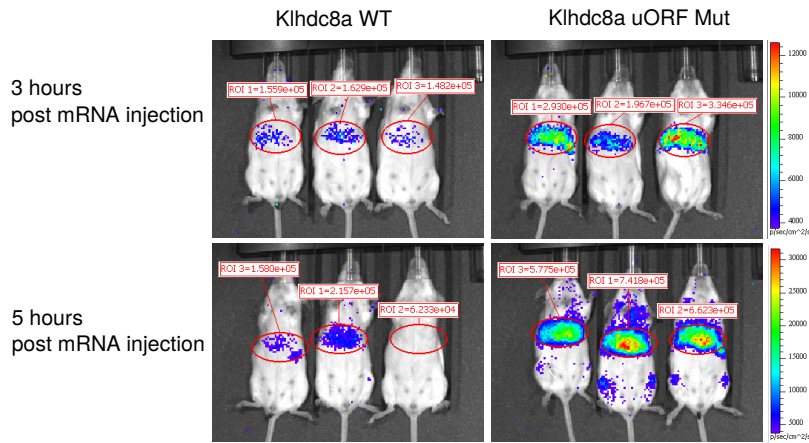


Supplementary Figure 4. Analysis of differential TE genes. **A)** Triplet periodicity of ribosome footprints within translated uORFs. Genes containing a single uORF were included in the analysis (n = 1154 genes/uORFs) to avoid uORFs overlapping to each other. **B)** Proportion of translated uORF-containing genes – specified as non-overlapping uORFs only, overlapping uORFs only, or both – transcriptome-wide (all translated) and among DENR targets (differential TE). The latter showed a depletion of overlapping uORFs and enrichment for genes containing only non-overlapping uORFs. **C)** Histogram of 5' UTR-to-CDS translation between *Denr* Kd and control cells, for all uORF-containing genes (grey, n=3688) and for differential TE genes (orange, n=186). Genes with a minimum of 20 RPF-seq reads in the 5' UTR in 3/4 of samples were included in the analysis. **D)** Same as in (C) for RNA-seq reads. Differential TE genes showed increased relative 5' UTR translation, but equal transcript levels, in *Denr*-deficient cells, that was higher than for the whole set of uORF-containing genes, suggestive of impaired translation reinitiation among targets. **E)** Gene Ontology (GO) analysis for Biological process, Metabolic function and Reactome functional categories of genes with differential TE. Bars show $-\log_{10}$ for categories with an $FDR < 0.05$.

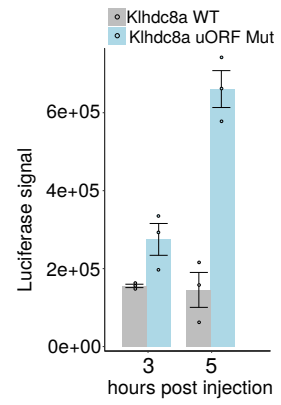


Supplementary Figure 5. Examples of differential TE genes. **A)** Representative examples of genes with differential TE. Panels show average CDS translation efficiency in control (grey) and *Denr* Kd (red) cells. **B)** *Denr* Kd-to-control translation on the 5' UTR (brown) and on the CDS (grey). DENR targets showed decreased CDS TE (A) and increased 5' UTR translation concomitant with reduced CDS translation in *Denr*-deficient cells. **C)** Normalized RPF (blue) and RNA (orange) read count distribution on several DENR targets, in knockdown (top) and control (bottom) cells. Different blue and orange shadings correspond to each replicate per condition. The first 1000 nt of the CDS are shown. Coloured boxes below profiles indicate translated uORFs. **D)** (Left) Quantification of translation efficiency on *Atf5* uORFs and main CDS, in control (grey) and *Denr*-deficient (red) cells. Dots represent replicate samples, error bars indicate mean \pm sd, and p-values are derived from t-test. (Right) As in (C), for *Atf5*. **E)** As in (D), for *Atf4*. **F)** (Top) Schematic representation of the dual luciferase reporter construct, in which the uORF stop codon was mutated so that the uORF translates into the CDS, in a different frame. These constructs allow testing the dependence on a functional stop codon for DENR-mediated regulation. Of note, if the function of DENR consisted in regulating the efficiency of uORF start codon selection, mutating the uORF stop codon should not have an influence on the DENR-effect in the reporter assay. (Bottom) Results of dual luciferase assay in control (grey) and *Denr*-depleted cells (red). Removal of the stop codons of *Clock*, *Klhdc8a* and *Etaa1* uORFs led to loss of DENR-dependence, indicating that the presence of a stop codon is necessary for DENR action, in line with a role of DENR as a reinitiation factor rather than a leaky scanning factor. FL signal was internally normalised to RL expressed from the same bidirectional promoter. FL/RL signals were normalised to the Scr-transduced non-mutated ("WT") vector. Signals from all *Denr*-shRNA transduced constructs were also normalised to the signal obtained for "empty vector, *Denr*-shRNA", to remove DENR effects that were not specific to the 5' UTR.

A

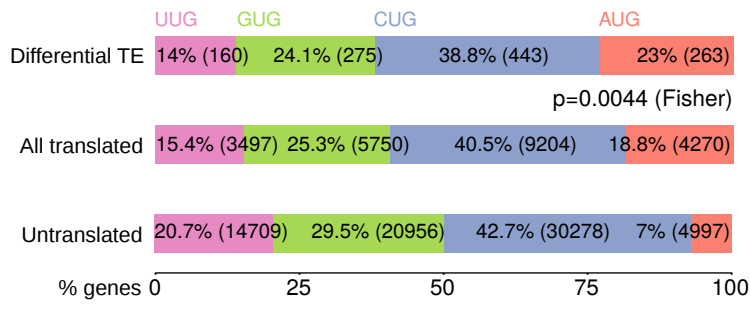


B

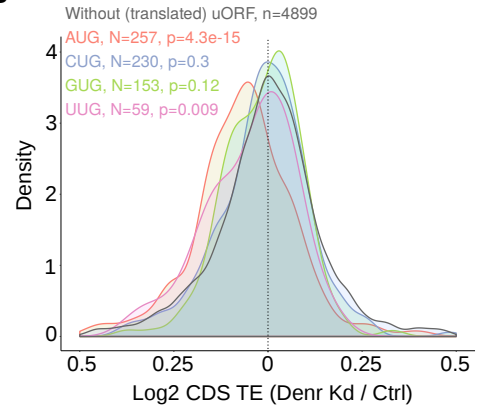


Supplementary Figure 6. In vivo-bioluminescence imaging. **A)** Synthetic mRNA with a WT or mutated *Klhdc8a* 5' UTR and being fully substituted with N1-methyl pseudouridine (to avoid induction of type I interferon *in vivo*) was injected intravenously in mice using a formulation that allows expression of the *in vitro*-transcribed mRNA primarily in the liver. The luciferase activity was recorded *in vivo* 3 and 5 hours after the injection of RNA. Numbers indicate radiance in the region of interest (ROI). **B)** Quantification of the bioluminescence experiments in A. Error bars indicate mean \pm sd.

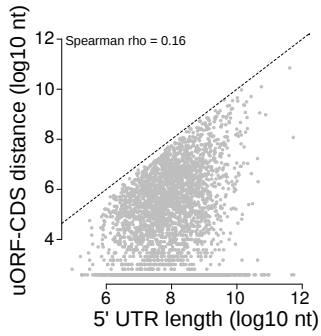
A



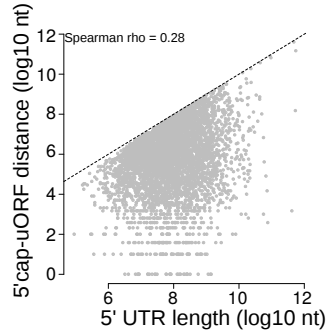
B



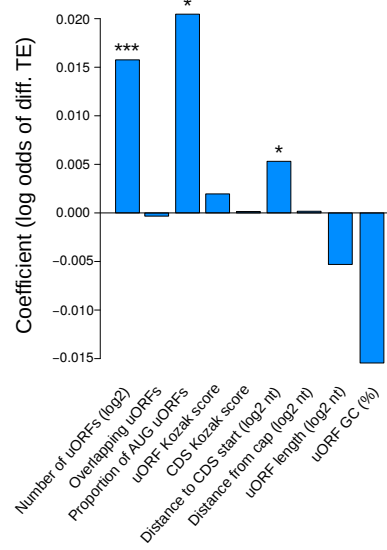
C



D

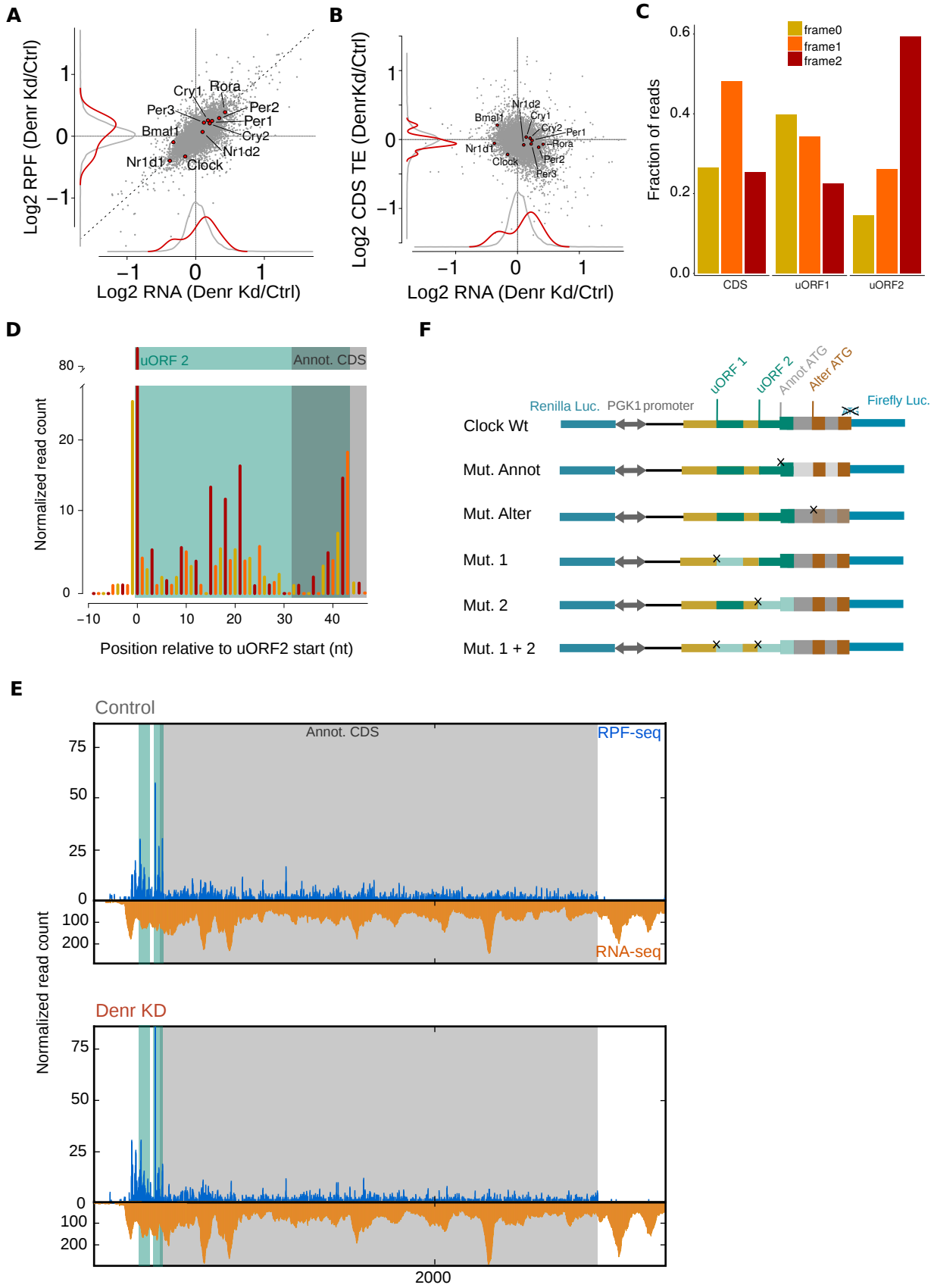


E



Supplementary Figure 7. Regression analyses of TE regulation by DENR.

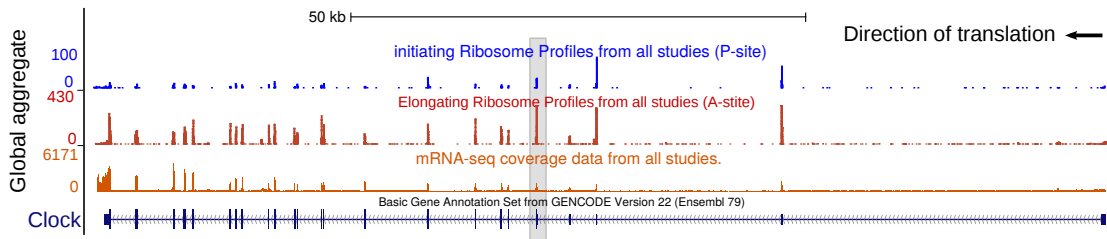
A) Proportion of AUG, CUG, GUG, and UUG uORFs detected as translated, un-translated and among differential TE genes. DENR targets are enriched for translated AUG uORFs ($p = 0.0044$, Fisher test), indicating start codon specificity among DENR-regulated transcripts. **B)** Density plot of the CDS TE ratio (*Denr* Kd/control) for genes containing only AUG ($n = 257$), only CUG ($n = 230$), only GUG ($n = 153$), or only UUG ($n = 59$) uORFs. P-values indicate Wilcoxon test results for the difference between each distribution and that of genes without uORFs (or with untranslated uORFs) ($N = 4899$). Although the number of genes per category is low, this analysis shows that AUG-containing genes have the strongest CDS TE regulatory effect upon *Denr* knockdown. **C)** Scatter plot of 5' UTR length vs. the distance from the last uORF stop codon to the CDS start for all uORF-containing genes used for the regression model. No strong correlation was quantified between the two variables, ruling out that the correlation of the intercistronic distance with the magnitude of DENR regulation was due to longer 5' UTRs. **D)** Scatter plot of 5' UTR length vs. the distance from the 5' cap to the first uORF start codon for all uORF-containing genes used for the regression model. No strong correlation was quantified between the two variables, but correlation was higher than in (C). **E)** Coefficients for the logistic regression model, with “detected as differential TE, TRUE/FALSE” as binary response. Coefficients thus indicate the log odds change for being detected as differential TE (by Xtail) per unit change in the predictor. Same genes as for Figure 4 were used. Asterisks indicate coefficient estimates significance as: $p < 0.05$ (*), $p < 0.01$ (**), $p < 0.001$ (***)).



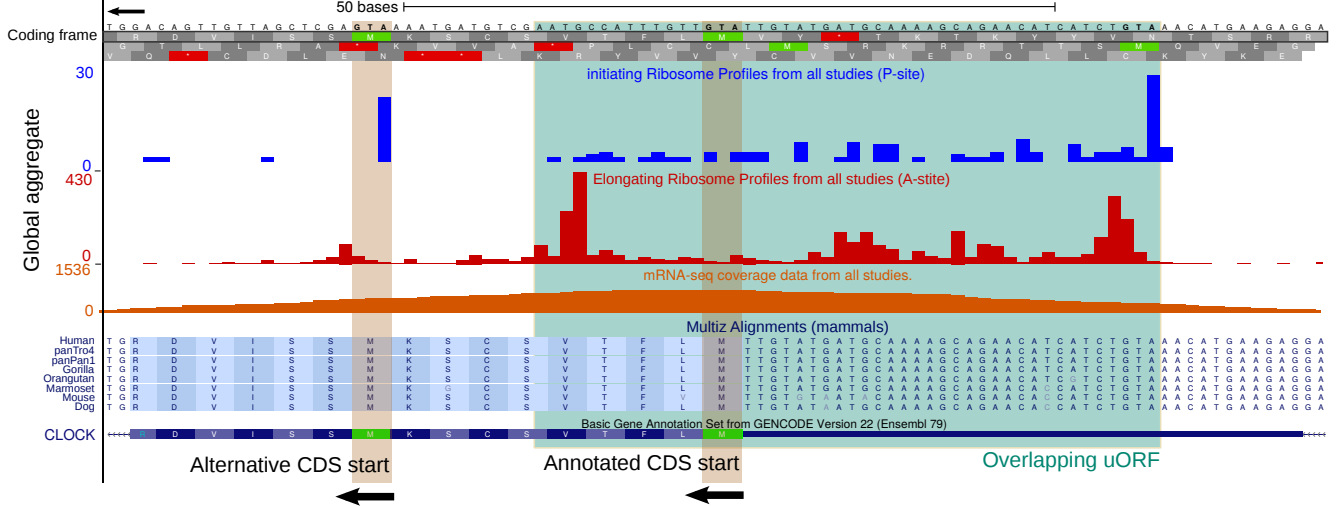
Supplementary Figure 8. Clock is a DENR target. **A)** Scatter plot of *Denr* Kd-to-control transcript levels (RNA-seq) vs. footprint levels (RPF-seq), with circadian core clock genes highlighted. *Clock* showed decreased translation without changes in mRNA abundance. **B)** Scatter plot of *Denr* Kd-to-control transcript levels (RNA-seq) vs. CDS translation efficiency, with circadian core clock genes highlighted. **C)** Frame preference of RPF-seq reads of *Clock* CDS, and both AUG uORFs. Frame preference within uORFs is similar to that on the CDS. **D)** Triplet periodicity within the uORF2. **E)** Distribution of normalised RPF-seq (blue) and RNA-seq (orange) reads along the *Clock* transcript, in control (top) and *Denr* Kd (bottom) cells. Green shaded area indicates the AUG-initiated uORFs; grey area corresponds to the annotated CDS. Only the first 500 nt of the 3' UTR are shown for better visualisation. **F)** Schematic representation of the *Clock* wild-type and mutant constructs tested for effect on reporter synthesis and DENR dependence. The *Clock* reporters contain the whole 5' UTR and the first 14 annotated amino acids of the CDS, in fusion with Firefly luciferase cDNA from which the start codon was removed. In addition, combinations of the mutated sites were cloned.



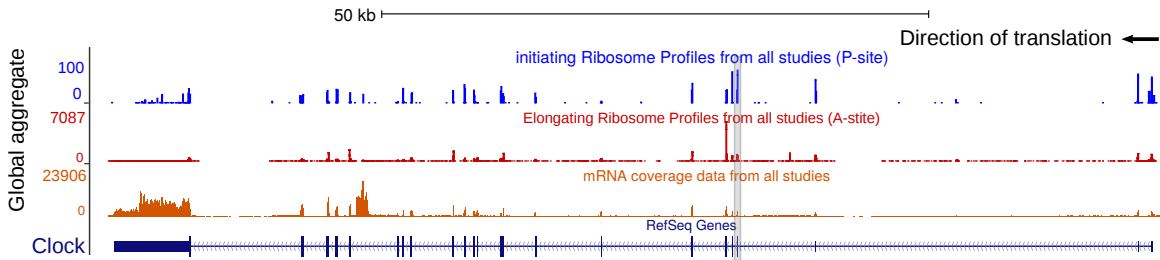
Human Dec. 2013 (GRCh38/hg38) chr4:55,426,793-55,547,902 (121,110 bp)



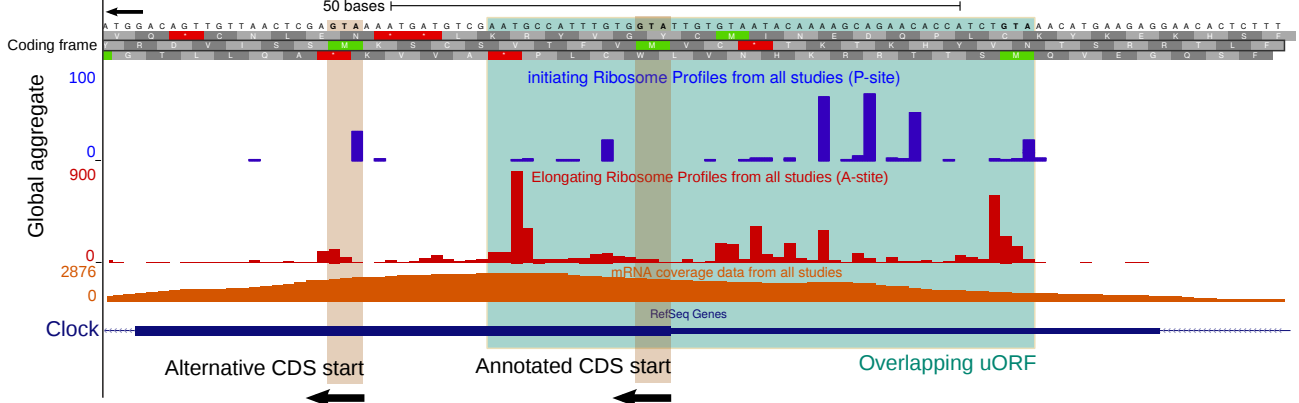
Human Dec. 2013 (GRCh38/hg38) chr4:55,482,733-55,482,836 (104 bp)



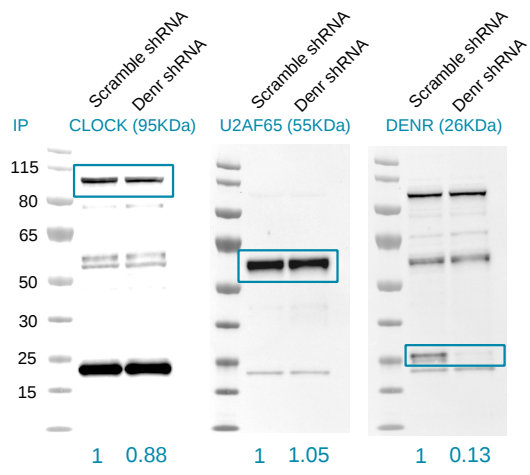
Mouse Dec. 2011 (GRCm38/mm10) chr5:76,208,184-76,310,458 (102,275 bp)



Mouse Dec. 2011 (GRCm38/mm10) chr5:76,266,788-76,266,906 (119 bp)



Supplementary Figure 9. Clock ribosome profiling data from published studies are consistent with alternative initiation from a downstream in-frame AUG. All available data from initiating and elongating ribosome profiling studies, gathered from GWIPS-viz (46). An overview of the whole *Clock* transcript and a zoom over the CDS start is shown, where reads mapping on the overlapping uORF (over green background) and annotated and alternative CDS starts are visualised. Both human (top) and mouse (bottom) data are displayed. Initiating ribosomes can be seen at the start of the uORF and alternative CDS start. Elongating ribosome data (similar to our study) show good uORF coverage.



Supplementary Figure 10. Reduced CLOCK protein levels in *Denr*-depleted cells. Left panel: Analysis of CLOCK levels in cells depleted of *Denr*. Middle panel: Same membrane probed against protein U2AF65, to assess equal loading. Right panel: Same membrane probed against DENR, indicating efficient knockdown. Numbers in blue indicate quantification of the signal using ImageJ, with Scramble shRNA-treated cells set to 1.